Dependence of Turbulent and Mesoscale Velocity Variances on Scale and Stability

L. MAHRT, ERIN MOORE, AND DEAN VICKERS

College of Oceanic and Atmospheric Sciences, Oregon State University, Corvallis, Oregon

N. O. JENSEN

Meteorology and Wind Energy Department, Risø National Laboratory, Roskilde, Denmark

(Manuscript received 11 February 2000, in final form 12 July 2000)

ABSTRACT

The scale dependence of velocity variances is studied using data collected from a grassland site, a heather site, and four forested sites. The dependence of velocity variances on averaging time, used to define the fluctuation quantities, is modeled. The crosswind velocity variance is emphasized, because it is more difficult to model than the other two components and is crucial input for applications such as dispersion modeling. The distinction between turbulence and mesoscale variances is examined in detail. Because mesoscale and turbulence motions are governed by different physics, meaningful study of the behavior of velocity variances requires adequate separation of turbulence and mesoscale motions from data. For stable conditions, the horizontal velocity variances near the surface exhibit a spectral gap, here corresponding to a very slow or nonexistent increase of variance with increasing averaging time. This ''gap region,'' when it occurs, allows separation of mesoscale and turbulence motions; however, the averaging times corresponding to this gap vary substantially with stability. A choice of typical averaging times for defining turbulent perturbations, such as 5 or 10 min, leads to the capture of significant mesoscale motions for very stable conditions and contributes to the disagreement with turbulence similarity theory. For unstable motions, the gap region for the horizontal velocity variances shrinks or becomes poorly defined, because large convective eddies tend to ''fill in'' the gap between turbulence and mesoscale motions. The formulation developed here allows turbulence and mesoscale motions to overlap into the same intermediate timescales. The mesoscale variances are less predictable, because a wide variety of physical processes contribute to mesoscale motions. Their magnitude and range of timescales vary substantially among sites. The variation of the behavior of turbulence variances among sites is significant but substantially less than that for the mesoscale motions.

1. Introduction

Turbulent variances and kinetic energy have been successfully approximated by turbulence similarity theory, although differences exist between studies. Discrepancies are greatest for very stable conditions. Existing formulations poorly describe mesoscale variations for all stability classes. Smedman (1988) finds that mesoscale motions do not obey Monin–Obukhov similarity theory, and their inadvertent inclusion in the turbulence variances degrades the performance of similarity theory. For example, the standard deviations of the velocity components scaled by the surface friction velocity are thought to be approximately constant for a given averaging scale for weak and moderate stability (Nieuwstadt 1984; Smedman 1988; Stull 1988; Sorbjan 1989). However, for very stable conditions, the scaled standard deviation of the velocity components can increase substantially with increasing stability (Smedman 1988). This increase is due to the decrease of the friction velocity and the increase of the relative contribution of the mesoscale motions to the computed variance for a fixed averaging time (Mahrt et al. 1998). Failure to separate turbulent and mesoscale motions may have contributed to deviations from Monin–Obukhov similarity theory for very stable cases in previous studies. Systematic measurement loss of flux (Howell and Sun 1999), flux sampling errors, and nonstationarity of the turbulence variance due to mesoscale modulation of the turbulence may also contribute to deviations from similarity theory.

The crosswind (perpendicular to the wind) velocity variance is the most difficult component to model, for reasons outlined in section 4e. Estimation of the crosswind velocity variance is important for applications such as dispersion models (Kristensen et al. 1981; Hanna 1983; Skupniewicz 1987; Lyons and Scott 1990). The standard deviation of the crosswind velocity variance

Corresponding author address: Larry Mahrt, College of Oceanic and Atmospheric Sciences, Oregon State University, Corvallis, OR 97331.
E-mail: mahrt@oce.orst.edu

can be sensitive to the range of scales included in its calculation. Correspondingly, the measurement of plume spread is sensitive to the choice of averaging time (Eckman 1994).

The mesoscale variances must be formulated separately from turbulence variances because their physics is different. When simultaneously considering a variety of sites and flow situations, a precise definition of mesoscale motions is not possible. Here, mesoscale motions are considered to be those motions that generally occur on scales larger than turbulent scales and do not obey turbulence scaling laws. The separation between the largest scale mesoscale motions and synoptic scale motions is not required for this study. Mesoscale motions in the nocturnal boundary layer include internal gravity waves, pulsating drainage flows (Doran and Horst 1981; Mahrt and Larsen 1982), vortical modes or fossil turbulence (Riley et al. 1981; Lilly 1983; Kristensen et al. 1981; Ruscher and Mahrt 1989; Gibson 1987), wake vortices (Etling 1990; Lilly 1983), and possible motions caused by a variety of other instabilities (Emanuel 1983). Except in the case of *well-defined drainage flows* or *monotonic gravity wave trains*, it has not been possible to isolate these motions uambiguously from atmospheric data. The vortical modes are primarily two-dimensional (vertical vorticity) and probably contribute substantially to horizontal meandering of plumes of pollutants (Hanna 1986). The term ''meander'' is not precisely defined. In dispersion studies, meandering may be identified with single particle diffusion or absolute dispersion. Shifting of the wind direction may also be caused by intermittent mixing in the stable boundary layer in the presence of vertical directional shear.

Vertical directional shear in the nocturnal boundary layer effectively disperses contaminants in different directions and misaligns the stress and shear directions. Such directional shear can be induced by cold air drainage at the surface and low-level jets at the top of the surface inversion layer (Moran and Pielke 1996). On a shorter timescale, meandering mesoscale motions more or less confined to separate layers may lead to substantial local directional shear.

The role of wake vortices (e.g., Arya et al. 1987) on dispersion and generation of turbulence is also poorly understood. Wake vortices may explain the greater variance of wind direction in complex terrain compared to uniform terrain, as observed by Moore et al. (1988), Chimonas (1999), and others.

Partitioning of the motion into mesoscale and turbulent contributions seems semitractable for stable conditions near the surface due to a scale gap between turbulent and mesoscale motions in the spectra for the horizontal velocity components near the surface for many flow situations (Smedman and Högström 1975; Caughey 1977; Olesen et al. 1984; Smedman 1988; Howell and Sun 1999; Högström et al. 1999, their Fig. 11). The existence of the spectral gap depends on the general flow regime and type of spectral plot and is more likely to occur close to the surface. Note that the spectral gap discussed here is between the mesoscale and turbulent scale. A gap between turbulent and synoptic scales due to lack of energy in the mesoscale range is generally not observed in the boundary layer, and the mesoscale regime seems to merge smoothly into the synoptic regime. Olesen et al. (1984) have modeled the timescale of the spectral gap between mesoscale and turbulent scale. When the source of turbulence is mesoscale instability, as in flow over complex terrain, a spectral gap may not occur (Mahrt and Gamage 1987).

On mesoscales, the spectral energy of the horizontal velocity components generally increases with increasing scale while that of the vertical velocity component is very small and decreases with increasing scale. Smith and Mahrt (1981) show that inhibition of mesoscale vertical motions by hydrostatic pressure adjustments in stratified flow increases with the scale of the horizontal motion.

Although mesoscale motions are generated in the boundary layer by a variety of mechanisms, several previous studies have attempted to model the spectra of mesoscale motions. Olesen et al. (1984) discount the spectral model developed by Weinstock (1980) for application to near-surface flows and derive a model of spectra for the horizontal mesoscale motion with a slope of -2. They point out the need for better observational validation. Stull (1988) includes a brief discussion of the physics and assumptions behind the -2 regime and additional references. Individual spectra may vary substantially among different situations. For example, SethuRaman (1977) found a mesoscale spectral peak in all three velocity components corresponding to gravity wave motion. Hanna (1983) found a dominant oscillation in the horizontal wind at a timescale of about 2 h.

Existing spectra of the velocity components in the literature imply how the variances should depend on averaging time, but existing spectral models cannot be integrated to provide an analytical expression for the velocity variances as a function of averaging time. Furthermore, integration of Fourier spectra over a given bandwidth does not satisfy Reynolds averaging. In this study, we concentrate on modeling the variances directly as a function of averaging scale. Given the variety of mesoscale motions, we cannot expect a simple model for the scale dependence of the velocity variances to be accurate. Nonetheless, some approximate model of the variances, which includes mesoscale motions, is required, because the influence of mesoscale meandering is considered to be important and suitable models currently do not exist. Although we address the full stability range, our emphasis is on the stable boundary layer where existing models are expected to be less accurate.

2. The data and basic analysis

Often conclusions based on one dataset are strongly influenced by features unique to that particular site. Con-

sequently, analysis of a single dataset has sometimes led to misleading conclusions. Therefore, this study includes data from six different field programs.

The first dataset is eddy correlation data from a Kaijo Denki, Inc., omnidirectional sonic anemometer at 39 m above ground over a 21-m-high aspen canopy in the boreal forest of Saskatchewan, Canada, from 3 February to 18 September 1994 (Blanken et al. 1997, 1998; Mahrt et al. 2000).

During Borris95, 7–14 July 1995, eddy correlation data were collected at 2, 7, 10, and 20 m above a low heather canopy in the Borris Moor of the Jutland Peninsula in Denmark. The sonic anemometers were Kaijo Denki except for a Gill, Ltd., Solent sonic anemometer at 7 m.

Eddy correlation data were collected with a Gill Solent sonic anemometer at 43 m over a 25-m-high uniform beech forest canopy in south central Sjaelland in Denmark (Pilegaard et al. 2000) as a Euroflux station. A second sonic anemometer dataset over a uniform beech forest was collected on Falster Island, Denmark, 23 February–29 April 1994. This study analyzes Gill Solent sonic anemometer data from 53 m above the 24-m-high canopy.

Eddy correlation data were collected with a Campbell Scientific, Inc., CSAT-3 sonic anemometer at 6.1 m above a 2-m sparse, semiarid ponderosa pine forest near Sisters, Oregon, from 1 to 27 June 1999 as an Ameriflux station. This is the only dataset analyzed in this study from complex terrain.

The final sonic anemometer (ATI, Inc., K probes) dataset was collected at 3 and 10 m over grassland in south central Kansas during Microfronts, 22 February–31 March 1995, (Sun 1999; Howell and Sun 1999; Mahrt et al. 1998). The grass was generally thick, permanently bent over, and matted. The average grass height was 25 cm above the ground surface. All of the datasets were quality controlled following the method of Vickers and Mahrt (1997). For each tower site, data corresponding to wind directions through the tower are masked out.

For some analyses, the Microfronts grassland data will be emphasized, because Microfronts has the simplest canopy. The data are partitioned into 4-h records: 1500–1900, 1900–2300, 2300–0300, 0300–0700, 0700–1100, and 1100–1500 local time. Modeling the turbulence in terms of 1-h records would be preferable in order to reduce the influence of nonstationarity; however, modeling the turbulence scales separately would require undesirable matching to the mesoscale regime.

Velocity fluctuations are computed as

$$\phi' = \phi - \overline{\phi}, \tag{1}$$

where the overbar represents averaging over a time period of τ. Modeling variances as a function of averaging time τ is a fundamental goal of this study. Instantaneous variances are then averaged over a longer averaging scale to produce

$$[\phi'^2], \tag{2}$$

where [ ] represent the longer term average, chosen to be 4 h in this study. The dependence of the variance on τ can be examined in terms of any arbitrary set of averaging scales. Here, we employ a dyadic series of averaging times, $\tau_m = 2^m$ points.

The variances, so computed, correspond to the integral of the multiresolution spectra (a form of wavelet spectra that satisfies Reynolds averaging) (e.g., Howell and Mahrt 1997), although we compute the variances directly without using spectra as an intermediate step. A gap in the multiresolution spectra, by definition, corresponds to a slow or nonexistent increase of the variance with increasing τ_m. We will refer to such regions as the ''gap'' region, which will normally occur between the turbulence and mesoscale scaling regions. The spectral gap in the multiresolution spectra generally corresponds to a gap in Fourier space, which occurs at somewhat larger scales. We prefer the multiresolution spectra, because they are based on a local basis set, which does not require periodicity for interpretation.

All averages are simple unweighted averages in order to satisfy Reynolds averaging assumptions. The surface stress and buoyancy flux are evaluated from fluctuations about the 5-min time average. This choice seemed to be the best one in terms of minimizing loss of flux in unstable conditions and inadvertent inclusion of mesoscale flux in stable conditions. The sign of the mesoscale fluxes were not systematic and inadvertent inclusion of mesoscale fluxes does not significantly influence the results based on class-averaged fluxes. Ultimately, one wishes to compute fluxes from a variable averaging length associated with the gap in spectra of the horizontal velocity variances, when it occurs. Because this procedure would not be straightforward for unstable cases, we have chosen the simpler approach of constant averaging length for computing the fluxes. This choice did not significantly affect the results, because the fluxes due to the large-scale motions are very small, in contrast to the horizontal velocity variances. Nonetheless, the procedure is not self-consistent.

a. Compositing and scaling

The variance $[\phi'^2](\tau)$ for different 4-h records is composited for different stability classes, nominally chosen in terms of the stability intervals ($z/L < -0.2$), (-0.2, -0.05), (-0.05, 0.04), (0.04, 0.1), (0.1, 0.5), and (>0.5), where z is height and L is Monin–Obukhov length. The choice of these classes roughly provides a comparable number of observations in each class when considering all of the datasets. A minimum of five records are required for a given stability class at a given site before computing the composited scale dependence. Velocity variances are significantly correlated with the surface friction velocity, but variances scaled by the surface friction velocity can be affected by ratio aver-

aging problems. For example, the composite of velocity variances scaled by u_*^2 can be dominated by one or two cases where u_*^2 values are exceptionally small, partly due to random sampling errors. This situation leads to more erratic behavior between classes, as quantified by Eq. (4). To avoid this classical ratio averaging problem, the variances and the surface friction velocity are separately averaged over all of the records within a stability class. The composited variance is then divided by the composited square of the surface friction velocity.

Scaling τ with z/U, where U is wind speed, can be thought of as inclusion of the suspected increase of vertical velocity variance with height near the surface and application of a form of Taylor's frozen turbulence hypothesis. Eddies of a given spatial scale move past the tower more quickly with stronger airflow, so U/τ is an estimate of the horizontal length scale. Corrections to Taylor's hypothesis have been recently discussed in Peltier et al. (1996). Unfortunately, there is no way to correct Taylor's hypothesis in the mesoscale range in which wave motions may be semistationary or may propagate with phase speeds much different than the wind speed. Scaling with respect to height is not useful for the horizontal velocity variances in unstable conditions, which are thought to be relatively constant with height and scale with the boundary layer depth for unstable conditions (section 4f). We return to the scaling problem with analysis of observations in section 4.

The different scaling strategies are quantitatively evaluated in terms of their ability to collapse the data onto a single curve, which will be expressed in terms of the standard error. Here, we define a single measure of variability of the scale-dependent variances between the $i = 1, I$ records for a given class, over the range of timescales between m_1 and m_2. This measure is written as

$$E^2 = \frac{1}{m_2 - m_1} \sum_{m=m_1}^{m_2} \left(\frac{1}{I}\right) \sum_{i=1}^{I} \{[\phi'^2]_i(\tau_m) - \langle [\phi'^2](\tau_m)\rangle\}^2, \tag{3}$$

where the angular brackets define compositing over all of the variances within a given stability class, m is the averaging scale index defined in the preceding subsection, and m_1 and m_2 determine the range of averaging scales.

The analogous measure of variability of the composited variance between the stability classes or between different sites for a given stability class ($j = 1, J$) is defined as

$$E_2^2 = \frac{1}{m_2 - m_1} \sum_{m=m_1}^{m_2} \left(\frac{1}{J}\right) \sum_{1}^{J} \{\langle [\phi'^2]\rangle_j(\tau_m) - \langle\langle [\phi'^2](\tau_m)\rangle\rangle\}^2, \tag{4}$$

where the double angular brackets indicate an average of the class-composited variance over all of the classes.

In some cases, we will attempt to model the scale-dependent variance in terms of a simple function. The suitability of the model fit to composited variance will be assessed in terms of

$$E_3^2 = \frac{1}{M} \sum_{m=m_1}^{m_2} (\text{Observed} - \text{Model})^2, \tag{5}$$

where $m = m_1, m_2$ are the different averaging scales. These three measures along with other considerations will be used (section 4) to assess the usefulness of scaling and modeling the velocity variances.

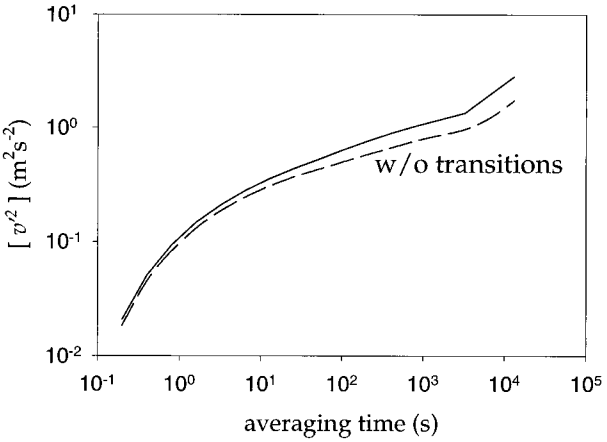

FIG. 1. Composited crosswind variances, with (solid) and without (dashed) the transition periods, for the grassland site.

b. Transition periods

The variance of the horizontal velocity components for averaging times greater than 2 h is larger during the morning (0700–1100) and late-afternoon transition periods (1500–1900) on some of the days with large diurnal variation. Part of the larger scale variance during these transition periods is associated with diurnal variation. Of all of the sites analyzed, the grassland site has the most pronounced diurnal cycle. For this site, excluding the transition periods reduces the average mesoscale crosswind variance (Fig. 1). However, much of this reduction is due to two cases of large change of the wind vector during the evening transition, one of which was associated with a frontal passage.

Attempting to filter out significant diurnal variation of the wind field during transition periods is an ambiguous process. Removing a higher-order fit to the trend for a given record also removes some of the transient mesoscale motion on larger scales. Removing the diurnal cycle composited over all of the days creates ambiguity for the meaning of the fluctuating wind component, because the diurnal variation of wind is not very systematic between days, in contrast to temperature. Here, no attempts are made to filter out diurnal effects. In fact, inclusion of the diurnal variation of the wind vector is required to model the total dispersion on timescales of several hours.

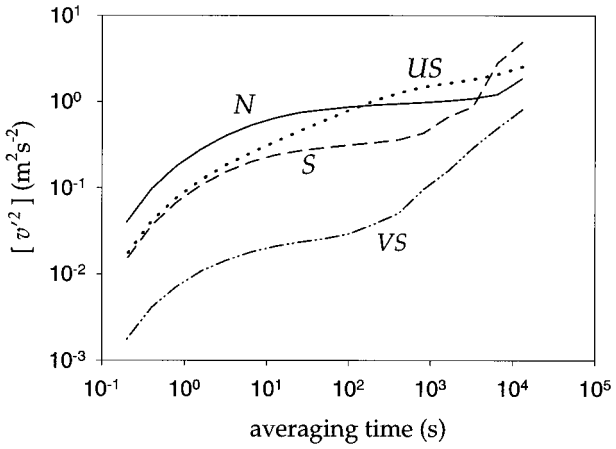

FIG. 2. Composited crosswind variances for the grassland site for the stability classes: very stable (VS) $z/L > 0.5$, stable (S) $0.1 < z/L < 0.5$, near-neutral (N) $-0.05 < z/L < 0.04$, and unstable (US) conditions $z/L < -0.2$.

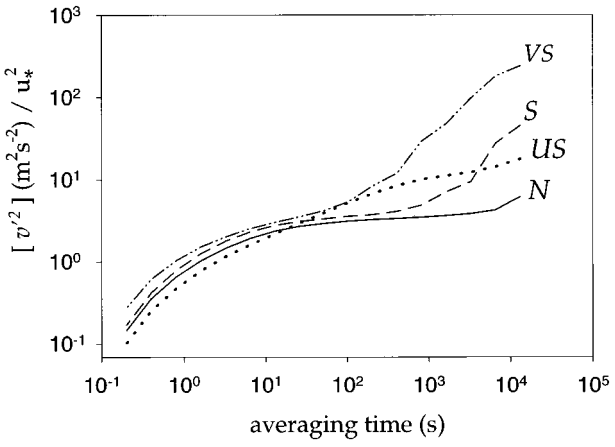

FIG. 3. Same as Fig. 2 except the crosswind velocity variance is scaled by the surface friction velocity.

3. Crosswind variance

a. Dependence on averaging time

For the Microfronts grassland site, the velocity variances, composited for individual stability classes (Fig. 2), increase rapidly with averaging time at small averaging times because of the inclusion of more turbulence with increased averaging time. Recall that τ defines the fluctuations, and the variances of the fluctuations are then averaged over 4-h periods. The gap between turbulent and mesoscale motions is indicated by the intermediate scale regime where the variance is essentially constant or increases only slowly with increasing averaging time (Fig. 2), corresponding to a minimum in the spectral density (section 2). The gap is best defined for stable conditions where the turbulence is confined to smaller scales. The very slow increase of the variance with increasing averaging time in the gap region implies that the variance is not sensitive to the choice of the averaging time τ, provided that τ is within the gap region. During evaluation of the turbulence similarity theory for the variances, one must choose averaging times corresponding to the gap region. However, the timescales corresponding to the gap region decrease substantially with increasing stability, implying that the averaging time defining turbulent fluctuations should decrease substantially with increasing stability. The turbulence extends up to only about $\tau = 100$ s in very stable conditions.

For the most unstable class, the turbulent scaling regime extends to 1 h or more for several of the sites, and the gap shifts to longer timescales (Fig. 2), as modeled by Olesen et al. (1984). With increasing instability, the large convective eddies ''fill in'' the gap for the horizontal velocity variances, and it becomes less well defined. The horizontal velocity fluctuations in this scale region seem to obey the same scaling as three-dimensional turbulence, but vertical velocity variance nearly vanishes. For unstable conditions, the vertical velocity variance normally reaches a near constant for timescales greater than 10 min. These large eddies on scales larger than 10 min may be roll vortices, inactive eddies (Högström 1990), or other eddies that appear to scale with the boundary layer depth, which will be subsequently referred to as ''large eddies.'' In terms of traditional definitions, these motions are not clearly turbulence or mesoscale motion.

Scaling the variance by the square of the surface friction velocity (u_*^2) substantially reduces the variation of the turbulent crosswind velocity variance between records for a given stability class for the turbulence scales and reduces the variation between composited values for the stability classes (Fig. 3). The turbulent scaling also partially reduced the variation of the velocity variances between classes for averaging times in the large-eddy region, although less so when compared with the small-scale turbulence. However, this scaling increased the difference between records and between stability classes in the mesoscale regime, implying that the mesoscale velocity variance is not related to the friction velocity in any systematic way. We return to the mesoscale regime in section 5.

b. Between-site variations

The scaled crosswind variance $[v'^2(\tau)]/u_*^2$ is generally smaller for forested sites as compared with short vegetation (Fig. 4). In comparison with short vegetation, the crosswind velocity variance over the forest does not increase as much as u_*^2 increases, even though scaling by u_*^2 does reduce the difference between forest and nonforested sites. The variation of $[v'^2(\tau)]/u_*^2$ between sites could be due to variation of typical wind speeds and boundary layer depth or differences between the height of the observations, as discussed in section 4f. The observational levels for some of the forest sites

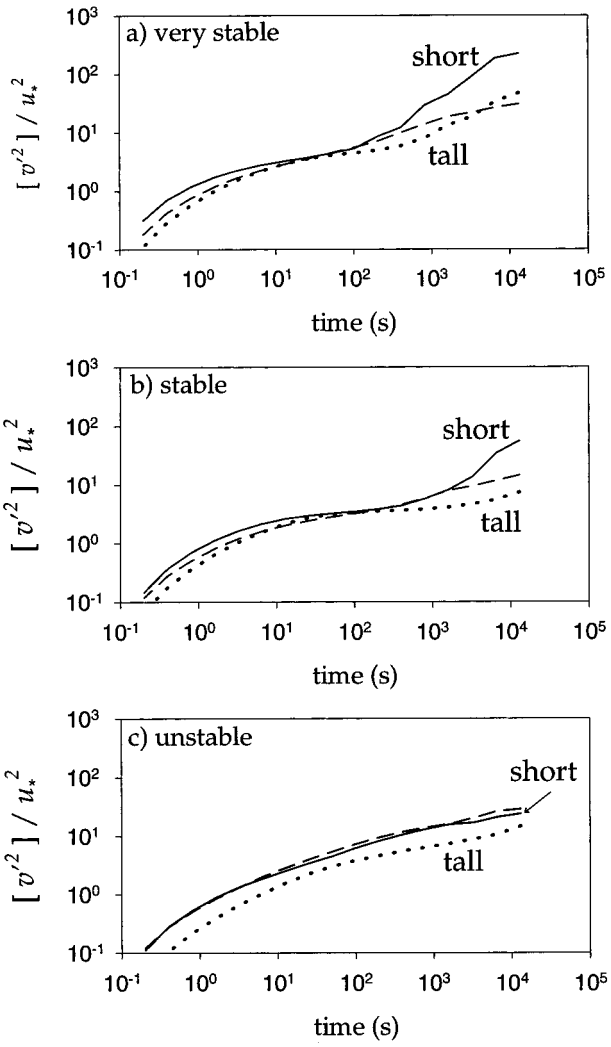

FIG. 4. Scaled composited crosswind variances for short vegetation (solid), tall vegetation (dotted), and the complex terrain example (dashed) for (a) the very stable, (b) stable, and (c) unstable classes.

may be in the roughness sublayer for unstable conditions (Nakamura and Mahrt 2000, manuscript submitted to *Bound.-Layer Meteor.*), which would contribute to the differences between the forested and short vegetation sites. The mesoscale variance differs much more between sites than the turbulence variance.

The variances for the ponderosa site did not follow the same pattern as the other forested sites. The ponderosa site is in complex terrain and is therefore not included in the forest composite. The composited variance for the ponderosa site is included as a separate curve (Fig. 4) but is not offered as a typical or representative case for complex terrain. Probably the mesoscale velocity variance is sensitive to the exact location with respect to terrain features. The crosswind velocity variance was generally not greater at the complex terrain site than at the other sites (Fig. 4). It may be that the valley setting restricted variation of wind direction, particularly at night when downvalley flow was often persistent.

4. Crosswind variance model

a. Model format

Our approach here is to model the turbulence part of the horizontal variance and then to model the residual from this expression as mesoscale motion. With this approach, mesoscale and turbulence motions may overlap in scale, as opposed to assuming all motions smaller (greater) than a certain scale are turbulent (mesoscale). If successful, this approach would reduce the contamination of the turbulence variances due to inadvertent inclusion of mesoscale motion in the turbulent velocity variance with fixed averaging times (see section 1).

Based on analyses detailed below, we model the crosswind velocity variance in terms of the overall function

$$[v'^2](\tau) = Cu_*^2\{1 - \exp[-(\tau/\tau^*)^n]\} + [v'^2(\tau_r) - Cu_*^2](\tau/\tau_r)^p, \qquad (6)$$

where the first term on the right-hand side models the turbulence contribution and the second term models the mesoscale contribution. (Here on the rhs the brackets have no special meaning.) The timescale τ^* (section 4c) and exponent n (section 4d) determine the scale dependence of the modeled turbulence variance. The stability-dependent coefficient C (section 4b) describes the amplitude of the turbulence variance relative to the surface friction velocity. For large averaging time with this model, the turbulence contribution to the variance asymptotes to Cu_*^2. The quantity Cu_*^2 determines the total turbulent crosswind velocity variance. For applications at levels that are not low in comparison with the boundary layer depth, one may wish to multiply the turbulence term by a function of height (section 4f). Such functions assume that the boundary layer depth is both definable and known.

The reference timescale τ_r will be chosen as 4 h in the analysis below. This defines the largest scale included in the mesoscale calculation, and the formulation in Eq. (6) is not valid for timescales greater than this value. The variance $[v'^2(\tau_r)] - Cu_*^2$ along with the exponent p determines the magnitude of the mesoscale variance (section 5). This procedure mathematically defines the mesoscale contribution. The physics remains unclear.

A comparison between the calibrated model [Eq. (6)] and the Microfronts data is shown in Fig. 5. The choice of the values of the coefficients for the turbulence contribution to the variance were guided by systematically varying n, C, and r^* and plotting the error [Eq. (5)] in $C - \tau^*$ space and in $n - \tau^*$ space for fixed values of the third variable. These plots offered guidance but did not clearly dictate a precise choice of the coefficients. The fit of the model to the observed variance considered

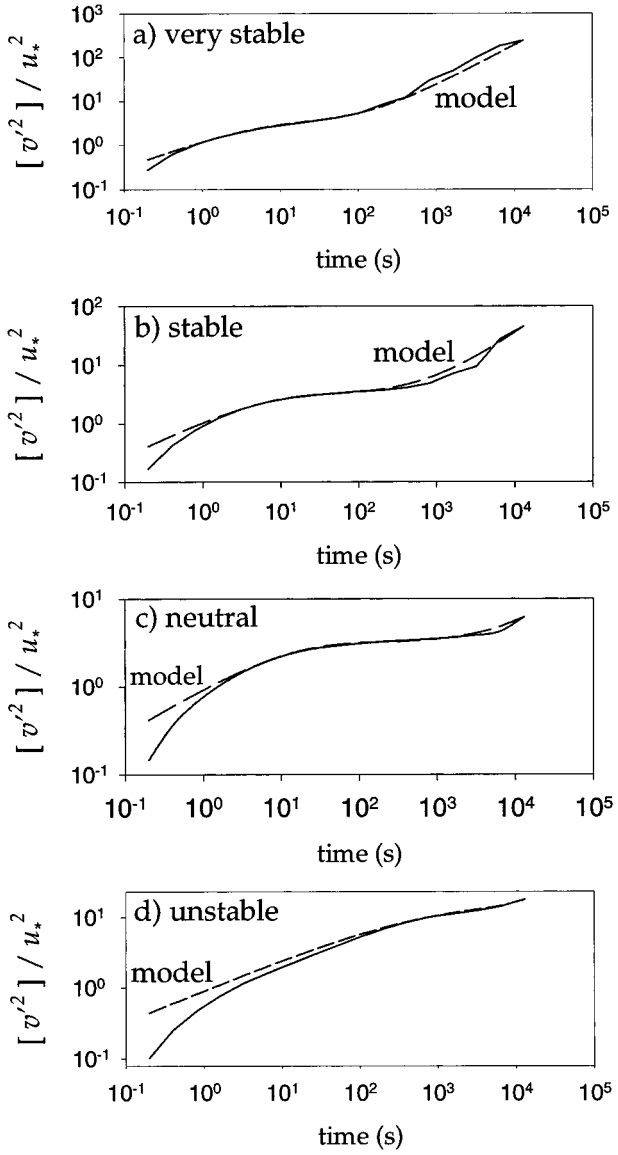

FIG. 5. Comparison of the model fit (dashed lines) with scaled composited crosswind variances (solid lines) for the grassland site for (a) the very stable, (b) stable, (c) near neutral, and (d) unstable classes.

the error over the range of timescales from the gap region down to small averaging times but ignored τ of a few seconds or less (Fig. 5), which are of limited practical application. The values of the coefficients chosen in the following subsections only apply for the range of stability represented by the data (e.g., Fig. 6).

b. The amplitude coefficient C

The coefficient C can be interpreted as the total nondimensional turbulence velocity variance $[v'^2]/u_*^2$, where the averaging operator [ ] is defined to be within the gap region. The value of C determined above increases significantly with increasing instability (Fig. 6) and increases more slowly with increasing stability. The large scatter in this figure and subsequent figures is partly due to combining data from widely different situations. The relationship for unstable conditions (Fig. 6) could be partly associated with expected correlation between boundary layer depth and z/L. Lumley and Panofsky (1964) noted that the scaled horizontal velocity variances do not vary significantly with height in the convective boundary layer (section 4e). The relationship of the variances to z/L was therefore due mainly to variations of L, not z. Wyngaard and Coté (1974) and Panofsky et al. (1977) formulate the standard deviation of the horizontal velocity components, scaled by surface friction velocity, as a function z_i/L, where z_i is the depth of the convective boundary layer. Panofsky et al. (1977) recommend for the unstable mixed layer

$$C = (12 - 0.5z_i/L)^{2/3}. \tag{7}$$

In Panofsky et al. (1977), this formulation applied equally well to either horizontal velocity component. In subsequent studies (e.g., Garratt 1992), the alongwind component was characterized by a larger value of C than for the crosswind component, as also occurs in the present data (section 6). The importance of the boundary layer depth is due to the contribution from large convective eddies, which scale with the boundary layer depth. Although the boundary layer depth generally increases with increasing instability $-z/L$, the boundary layer depth also depends on time history, stratification above the boundary layer, and large-scale subsidence. The variation of the dependence of $[v'^2]/u_*^2$ on z/L between sites in the current study may be partly due to differences of typical boundary layer depth between the sites.

For many applications, information on boundary layer depth is unavailable. For stable conditions, Eq. (7) may not apply (Garratt 1992), and, for very stable conditions, the boundary layer depth is not definable. To retain such situations, we consider a formulation for $[v'^2]/u_*^2$ based only on z/L. A subjectively determined fit to all of the datasets (Fig. 6, solid line) is expressed as

$$C = C_o\left(1 - a\frac{z}{L}\right)^q, \tag{8}$$

where $C_o = 2.6$. The exponent q is chosen to be 2.0 for unstable conditions and 1.0 for stable conditions, and a is equal to 1.0 for unstable conditions and 0.2 for stable conditions, where again this approximation is valid only for the range of stability in Fig. 6. Again, C is defined in terms of the estimated turbulent part of the velocity variance so that it is not exactly equal to $[v'^2]/u_*^2$ for any given averaging time.

In Smedman (1988), $[v'^2]/u_*^2$ increases sharply with z/L for stable conditions after z/L exceeds 0.5 (very stable conditions), apparently because of capture of me-

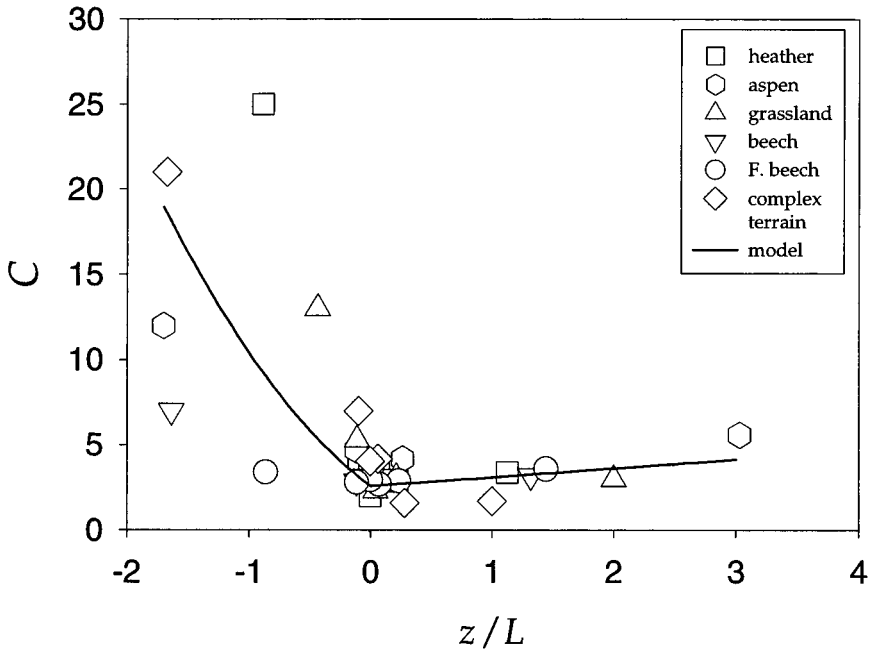

FIG. 6. Dependence of the coefficient C [Eq. (6)] on stability and the formulation for $C(z/L)$ [solid line; Eq. (8)].

soscale motions. Mahrt et al. (1998) found that decreasing the averaging time to 100 s for very stable conditions removed much, but not all, of the increase of $[v'^2]/u_*^2$ with increasing z/L. This averaging time roughly corresponds to the mesoscale end of the gap region for the present datasets for very stable conditions (Fig. 3). The fit based on Eq. (8) indicates that even after attempting to remove the mesoscale contribution to the velocity variance, the scaled velocity variance still increases slowly with z/L. Such an increase might be influenced by artificial correlations, since the surface friction velocity appears in the denominator of both the x and y axes. A constant value of $C = 2.6$ might suffice for practical applications. The above formulation for C ignores differences between sites (section 3b). The large scatter for the unstable case is probably due partly to the omission of information on the boundary layer depth.

c. The averaging timescale τ^*

The characteristic timescale τ^* increases with increasing instability corresponding to large eddies for very unstable conditions (Fig. 7) and decreases to very small values for strongly stable conditions corresponding to small eddies. Note that the characteristic timescale decreases substantially from slightly unstable conditions to slightly stable conditions. The characteristic timescale τ^* may also be sensitive to the horizontal wind speed, because eddies of a given size pass the tower more quickly with stronger winds. Therefore, the scaled variances are alternatively computed as a function of the pseudoaveraging length scale

$$L_\tau \equiv U\tau. \tag{9}$$

Although τ^* generally decreases with increasing wind speed for a given value of stability, expressing the horizontal velocity variance in terms of L_τ instead of τ did not reduce the differences between different sites, as evaluated from Eq. (4). Any advantage of expressing the variance in terms of the pseudoaveraging length instead of the timescale may be overshadowed by differences between sites. Relating the variance to the pseudoaveraging length did reduce the difference between individual records [based on Eq. (3)], for unstable conditions at a given site. Use of the pseudoaveraging length did not reduce the difference between records for stable conditions, even for a fixed site. For stable conditions, the size of the eddies apparently increases with wind speed, which partially offsets the influence of a shorter passage time with increasing wind speed for a given eddy size.

Here, we model the variance in terms of τ, which can be more directly applied. The dependence of τ^* on z/L (Fig. 7) is modeled as

$$\tau^* = \tau_o \exp(-bz/L), \tag{10}$$

where τ_o is 20 s and b is equal to 1.75 for unstable conditions and 0.95 for stable conditions.

d. The turbulence exponent n

The observations suggest a simple formulation in which $n = 0.5$ for unstable conditions and $n = 0.7$ for

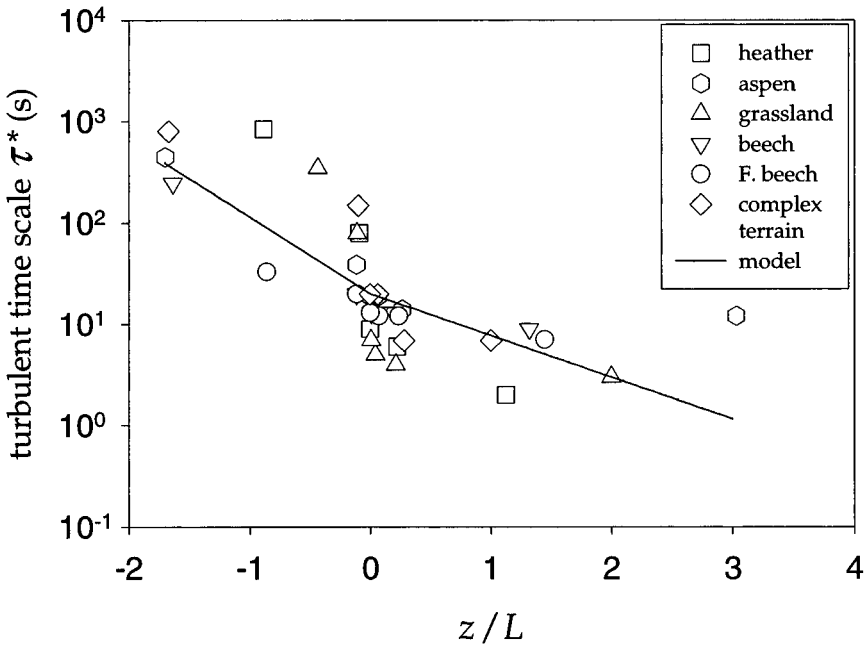

FIG. 7. Dependence of the turbulence scaling timescale τ^* [Eq. (6)] and the modeled value [Eq. (10), solid line] on stability.

stable conditions (Fig. 8). The smaller value of the exponent for unstable conditions corresponds to a more gradual approach of the turbulence variance to the gap regime (Fig. 8), which was less well defined in the unstable case.

e. Why large scatter?

If the conditions for Monin–Obukhov similarity are met, the scaled velocity variances should follow a universal dependence on stability. However, this relationship in the above figures exhibits large scatter. A number of factors contribute to this scatter.

1) The crosswind variance shows considerably more scatter than that for the other two velocity components. The crosswind variance is more vulnerable to nonstationarity. The influence of nonstationarity due to diurnal transition periods was shown in Fig. 1. We have not screened the data for nonstationarity in order to avoid creating a bias toward certain periods of the day and certain weather conditions.
2) The scatter for the turbulence range of scales is reduced by using 1-h records instead of 4-h records, which reduces the role of nonstationarity. We have used 4-h records to include a large range of scales without awkward matching between turbulence and mesoscale regimes.
3) We have combined data from different types of surfaces. The dependence of the scaled variances on stability at a given site is less. For example, the relationship of the scaled vertical velocity variance to the stability for the Microfronts grassland for 1-h records, after screening for nonstationarity, shows much less scatter (Mahrt et al. 1998) when compared with the above analyses based on data from a variety of sites for all conditions.
4) Our analysis indicates that some of the observations over the forested sites could be in the roughness sublayer where Monin–Obukhov similarity theory does not apply and additional scaling variables are required. For the unstable case, information on the boundary layer depth should be included.
5) For very stable conditions, Monin–Obukhov similarity theory is thought to break down for a variety of reasons (Mahrt 1999).

f. Height dependence

Only the heather and grassland sites have multiple observational levels above the roughness sublayer where the vertical structure can be examined. The grassland site has eddy correlation measurements at 3 and 10 m, and the heather site has observations at 2, 7, 10, and 20 m. One might have expected that the variance would decrease significantly with height across the tower in stable conditions due to thin boundary layers. However, the variance often increased with height, perhaps associated with generation of turbulence above the surface inversion, detached from the surface (Mahrt 1999). This is an example of ''*z*-less'' stratification (Wyngaard 1973), for which the height above ground becomes irrelevant. In general, the height dependence of the turbulence variance was not systematic for stable conditions. For weakly stable windy conditions, the scaled

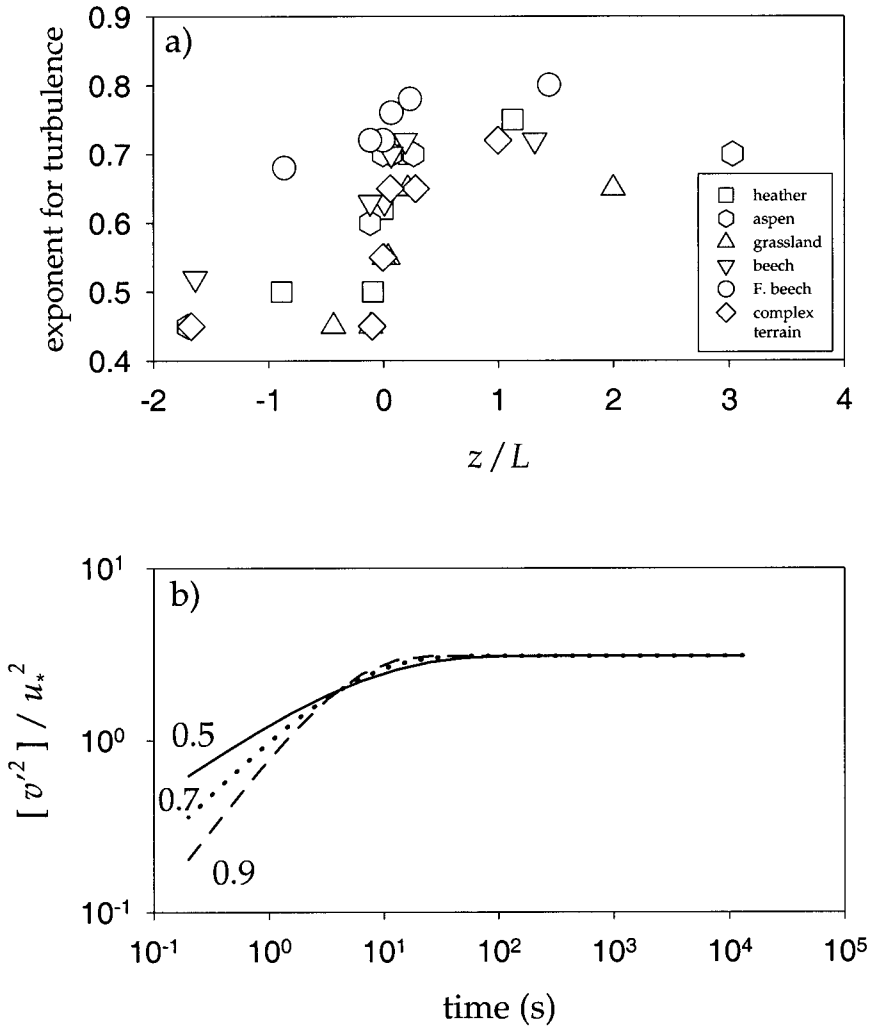

FIG. 8. (a) Dependence of the model exponent n [Eq. (6)] for crosswind turbulence on stability and (b) dependence of the modeled crosswind variance on the choice of n.

variances for all three velocity components were found by Lenschow et al. (1988) to decrease systematically with z/h, where h is the boundary layer depth.

For unstable conditions, the towers were too short for evaluation of the dependence on height in the boundary layer, and we must rely on the literature to complete this part of the variance model. For unstable conditions, the horizontal velocity variances tend to be more independent of height (Lumley and Panofsky 1964) because of dominance by convective eddies on the scale of the boundary layer. Rodean (1996) and Nasstrom et al. (2000) suggest a unified relationship of the simple form

$$[v'^2] = C(1 - z/h)^r u_*^2 + \beta w_*^2, \qquad (11)$$

where w_* is the convective velocity scale and β is a constant. In the convective case, the second term dominates and the scaled variance becomes approximately independent of height. In the absence of the convective term, the horizontal velocity variance decreases with height and vanishes at the boundary layer top. The exponent r varies between studies; Nasstrom et al. (2000) chose $r = 3/2$. Although this formulation does not match traditional Monin–Obukhov similarity theory as z approaches zero, it does provide suitable dependence on stability and a smooth transition between stable and unstable conditions.

Guided by Eq. (11), height dependence is incorporated into the first term on the right-hand side of Eq. (6) by choosing the format

$$C(z/L)u_*^2\{1 - \exp([\tau/\tau^*]^n)\}\, f(z/h), \qquad (12)$$

where $f(z/h)$ is $(1 - z/h)^{3/2}$. A more complete model would replace the exponent 3/2 with a stability-dependent exponent and allow for nonzero velocity variance at the boundary layer top. The influence of surface heating, represented by βw_*^2 in Eq. (11), is included in $C(z/L)$ (section 4b). Our data analysis did not find a

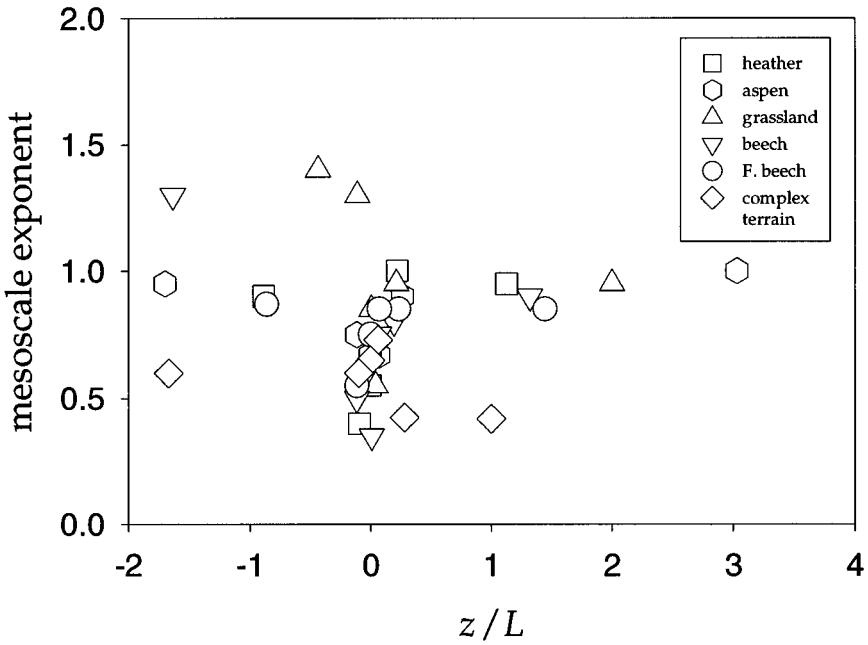

FIG. 9. Dependence of the exponent p for the crosswind mesoscale model [Eq. (6)] on stability.

clear dependence of the mesoscale variance on height, and the second term on the right-hand side of Eq. (6) remains independent of height.

5. Mesoscale crosswind variance

The mesoscale variance is not likely to follow simple scaling because mesoscale motions are generated by a variety of physical mechanisms (section 1). Indeed the exponent p for the crosswind mesoscale variance does not vary systematically with stability or vegetation type (Fig. 9). The value of the exponent p varies with the choice of τ_r, but the closeness of the model fit is not sensitive to this choice. Here, τ_r is 4h. Values of p greater than unity imply domination of the larger mesoscale motions on the scale of a few hours or more and a steeper increase of the mesoscale variance with τ at the larger scales. This case is observed for unstable conditions over the grassland and the Euroflux beech forest sites. Values of p significantly less than unity correspond to dominance by small mesoscales and slower increase of the variance at larger scales. This case occurs with near-neutral conditions at some of the sites. We recommend an average value of $p = 0.8$.

The model for the crosswind variance also requires specification of the amplitude of the mesoscale motion, $[v'^2](\tau_r) - Cu_*^2$. The magnitude of $[v'^2](\tau_r) - Cu_*^2$ might depend on the range of mesoscales permitted by the calculation. For strong stability, the turbulence is confined to small scales, permitting a large range of mesoscale motions between turbulent scales and the 4-h period. In contrast, for the most unstable class, the modeled turbulence captures most of the total variance until near the largest permitted values of τ, causing the range of captured mesoscale motion and the total mesoscale variance to be small. In spite of this influence, $[v'^2]$(4 hours) $- Cu_*^2$ shows no dependence on stability. Here, we choose an overall constant of $[v'^2]$(4 hours) $- Cu_*^2 = 0.6$ m^2 s^{-2}. Although the choice of a constant might be considered as a failure for the attempt to model the mesoscale variance, this procedure may be preferable to neglecting the influence of mesoscale motions or applying turbulence similarity theory to this range of scales.

For comparison, we also examined the mesoscale motion defined as the variance between two specified timescales, such as 30-min and 4-h averaging times, referred to as the ''fixed timescale approach.'' With this more traditional approach, the computed mesoscale variance may inadvertently capture some of the turbulence variance with unstable conditions and miss much of the smaller mesoscale variance with very stable conditions. This estimate of the mesoscale crosswind variance also shows little dependence on wind speed or stability.

Olesen et al. (1984) model the mesoscale spectra for stable conditions by appealing to earlier work of Lumley (1964) based on gravity wave considerations. Their formulation suggests that the mesoscale variance should increase with increasing stratification. Here, the stratification is most reliably computed from thermocouples employed above the heather site. For this site, the mesoscale variance did not show an obvious relationship to the stratification. Similarly, Högström et al. (1999) found no significant relationship between low-level horizontal velocity spectra and the Brunt–Väisälä frequency. In contrast, Caughey (1977) finds that the peak of

TABLE 1. Values of the model coefficients for the three turbulence velocity variances. Here C_o is the scaled amplitude of the turbulence variance; a (unstable/stable) and q (unstable/stable) are coefficients for the stability dependence; τ_o is the characteristic timescale of the turbulence for neutral conditions, expressed in seconds; b (unstable/stable) is the coefficient for variation of the characteristic timescale with stability; and n (unstable/stable) is the exponent coefficient for the turbulence velocity variance. The turbulent timescale τ^* is computed from Eq. (10) using values of τ_o and b.

Variable	C_o	a	q	τ_o	b	n
$[v'^2]$	2.6	1.0/0.2	2.0/1.0	20	1.75/0.95	0.7/0.5
$[\mu'^2]$	4.7	1.0/0.2	1.0/1.0	35	1.75/0.95	0.7/0.6
$[\omega']$	1.3	3.0/3.0	0.67/0.67	5	1.75/0.95	0.65/0.55

the mesoscale spectra scales with the Brunt–Väisälä frequency. The behavior of the mesoscale variance is situation dependent.

If at least part of the mesoscale crosswind variance for stable conditions is due to upscale energy transfer, as in formation of vortical modes, or if gravity waves are induced by turbulence vertical velocity fluctuations, then the mesoscale variance is physically related to the turbulence and friction velocity. When all of the datasets are considered, the mesoscale variance did not depend systematically on the surface friction velocity. The overall difficulty of predicting the mesoscale variance is probably partly due to the propagation of mesoscale motion from outside the observation region, including internal gravity waves and the onset of cold-air drainage (Blumen et al. 1999).

6. Model for the three velocity variances

The behavior of the alongwind and vertical-velocity variance is more similar between sites in comparison with the crosswind variance. The model parameters for the alongwind and vertical velocity components are determined in the same way as that outlined for the crosswind variance in the previous sections. The total model is Eqs. (6), (8), and (10), with the coefficients listed in Tables 1, 2.

Notice that the amplitude of the variance and the timescale are both largest for the alongwind variance and both smallest for the vertical velocity component (Table 1), consistent with traditional spectra (e.g., Kaimal and Finnigan 1994). The model coefficients for the scaled vertical velocity variance are based on Panofsky et al. (1977) (see also Merry and Panofsky 1976; Panofsky and Dutton 1984) and worked well for the short vegetation but tended to overestimate the scaled variance for the forest sites. The discontinuity of the exponent n (section 4d) is an oversimplification; however, more complex relationships must await further collection of data.

As with the crosswind variance, the height dependence for levels that are not small when compared with the boundary layer depth can be included by replacing the first term on the right-hand side of Eq. (6) with Eq. (12) for the alongwind variance, except using the coefficients for the alongwind variance from Table 1. The same height dependence is used for the vertical velocity variance for stable conditions. For the height dependence for the vertical velocity component for unstable conditions, one can use (e.g., Garratt 1992)

$$f(z/h) + (z/h)^{1/3}(1 - z/h)^{1/3}. \quad (13)$$

The mesoscale vertical velocity variance was small and was subject to significant relative errors in all of the datasets; it is set to zero in our model.

TABLE 2. Values of the model coefficients for the three velocity components for the mesoscale velocity variances, where p is the mesoscale exponent and meso − amp is the mesoscale amplitude $\{[\phi'^2]$ (4 hours) $- Cu_*^2\}$ (m^2 s^{-2}).

Variable	p	Meso − amp
$[v'^2]$	0.8	0.6
$[\mu'^2]$	0.7	0.6
$[\omega'^2]$	Na*	0.0

* Not applicable.

7. Conclusions and discussion

The above study analyzed data from six different field programs to form a model of the horizontal and vertical velocity variances as a function of the surface friction velocity, stability, and averaging time used to define the fluctuations. The model incorporates the dramatic change of turbulence scales with changing stability in order to better isolate turbulence and mesoscale motions. The mesoscale variance is mathematically defined by the procedures in section 4, which allows mesoscale and turbulence motions to overlap in scale. Traditional approaches, which use a constant averaging time or filter wavelength to define the perturbations for a range of stability, fail to separate turbulence and mesoscale horizontal velocity variances.

The mesoscale and turbulence motions seem most easily separated for stable conditions near the surface for which the horizontal variances are characterized by a spectral gap. This gap region reveals itself in the current study through a very slow or nonexistent increase of the velocity variance with increasing averaging time (section 2). The computed variances are not sensitive to the choice of averaging time for averaging times within the gap region. Traditional calculation of turbulent velocity fluctuations from data may inadvertently capture mesoscale variance for very stable conditions for which the gap region is shifted to very small timescales. Failure to separate turbulence and mesoscale motions in previous studies may have contributed to the breakdown of Monin–Obukhov similarity theory for velocity variances for very stable conditions.

In spite of this care in separating turbulence and mesoscales, the relationship between scaled velocity variances and stability shows large scatter even for the

turbulence range of scales, as is discussed in section 4e. We have concentrated on the crosswind variance, which is more vulnerable to nonstationarity and shows more scatter compared to the other two velocity components. To avoid bias, we have not screened for weather conditions or situations where similarity theory does not apply, and we have simultaneously included a wide variety of surface types. For a given site, the scatter is less.

The total model is summarized in section 6. This model is different from previous models in that it includes a specific dependence on averaging time and is based on a variety of surface conditions, including tall forest canopies. This model can be improved but at the expense of additional coefficients. Even then, a number of problems remain. The task of formulating universal relationships for a variety of surface types and weather conditions is problematic (section 4e). The use of a dimensional timescale to characterize the turbulence is undesirable, and the various influences on the characteristic turbulence timescale for stable conditions needs to be sorted out. The gap between mesoscale and turbulent motions is less well defined in unstable conditions. For very unstable conditions, an intermediate range of scales seems to follow the turbulence scaling for the horizontal variance, yet the vertical velocity variances are near zero. Here, separation of the motion into turbulence and mesoscale components is not obvious. Last, the mesoscale variances do not satisfy simple scaling and vary dramatically among different sites. An overall mean dependence of the mesoscale velocity variances on averaging time is provided here (Table 2).

Acknowledgments. The very useful comments of Zbigniew Sorbjan, Robert Grossman, and an anonymous reviewer are appreciated. This material is based upon work supported by Grant DAAD19-9910249 from the Army Research Office and Grant 9807768-ATM from the Physical Meteorology Program of the National Sciences Program.

REFERENCES

Arya, S. P. S., M. Capauno, and L. Fagen, 1987: Some fluid modeling studies of flow and dispersion over two-dimensional hills. *Atmos. Environ.,* **21,** 753–764.

Blanken, P. D., and Coauthors, 1997: Energy balance and canopy conductance of a boreal aspen forest: Partitioning overstory and understory components. *J. Geophys. Res..,* **102,** 28 915–28 927.

——, and Coauthors, 1998: Turbulent flux measurements above and below the overstory of a boreal aspen forest. *Bound.-Layer Meteor.,* **89,** 109–140.

Blumen, W., R. L. Grossman, and M. Piper, 1999: Analysis of heat budget, dissipation and frontogenesis in a shallow density current. *Bound.-Layer Meteor.,* **91,** 281–306.

Caughey, S. J., 1977: Boundary-layer turbulence spectra in stable conditions. *Bound.-Layer Meteor.,* **11,** 3–14.

Chimonas, G., 1999: Steps, waves and turbulence in the stably stratified planetary boundary layer. *Bound.-Layer Meteor.,* **90,** 397–421.

Doran, J. C., and T. W. Horst, 1981: Velocity and temperature oscillations in drainage winds. *J. Appl. Meteor.,* **20,** 360–364.

Eckman, R. M., 1994: Influence of the sampling time on the kinematics of turbulent diffusion from a continuous source. *J. Fluid Mech.,* **270,** 349–375.

Emanuel, K. A., 1983: On the dynamical definition(s) of ''mesoscale.'' *Mesoscale Meteorology—theories, Observations and Models,* D. K. Lilly and T. Gal-Chen, Eds., Reidel, 1–12.

Etling, D., 1990: On plume meandering under stable stratification. *Atmos. Environ.,* **24A,** 1979–1985.

Garratt, J. R., 1992: *The Atmospheric Boundary Layer.* Cambridge University Press, 316 pp.

Gibson, C. H., 1987: Fossil turbulence and intermittency in sampling oceanic mixing processes. *J. Geophys. Res.,* **92,** 5383–5404.

Hanna, S. R., 1983: Lateral turbulence intensity and plume meandering during stable conditions. *J. Climate Appl. Meteor.,* **22,** 1424–1430.

——, 1986: Spectra of concentration fluctuations: The two time scales of a meandering plume. *Atmos. Environ.,* **20,** 1131–1137.

Högström, U., 1990: Analysis of turbulence structure in the surface layer with a modified similarity formulation for near neutral conditions. *J. Atmos. Sci.,* **47,** 1949–1972.

——, A.-S. Smedman, and H. Bergström, 1999: A case study of two-dimensional stratified turbulence. *J. Atmos. Sci.,* **56,** 959–976.

Howell, J., and L. Mahrt: 1997, Multiresolution flux decomoposition. *Bound.-Layer Meteor.,* **83,** 117–137.

——, and J. Sun, 1999: Surface layer fluxes in stable conditions. *Bound.-Layer Meteor.,* **90,** 495–520.

Kaimal, J. C., and J. J. Finnigan, 1994: *Atmospheric Boundary Layer Flows: Their Structure and Measurement.* Oxford University Press, 289 pp.

Kristensen, L., N. O. Jensen, and E. L. Peterson, 1981: Lateral dispersion of pollutants in a very stable atmosphere: The effect of meandering. *Atmos. Environ.,* **15,** 837–844.

Lenschow, D. H., X. S. Li, C. J. Zhu, and B. B. Stankov, 1988: The stably stratified boundary layer over the Great Plains. I. Mean and turbulence structure. *Bound.-Layer Meteor.,* **42,** 95–121.

Lilly, D. K., 1983: Stratified turbulence and the mesoscale variability of the atmosphere. *J. Atmos. Sci.,* **40,** 749–761.

Lumley, J. L., 1964: The spectrum of nearly inertial turbulence in a stably stratified fluid. *J. Atmos. Sci.,* **21,** 99–102.

——, and H. A. Panofsky, 1964: *Structure of Atmospheric Turbulence.* Wiley Interscience, 239 pp.

Lyons, T., and B. Scott, 1990: *Principles of Air Pollution Meteorology.* CRC Press, 224 pp.

Mahrt, L., 1999: Stratified atmospheric boundary layers. *Bound.-Layer Meteor.,* **90,** 375–396.

——, and S. Larsen, 1982: Small scale drainage front. *Tellus,* **34,** 579–587.

——, and N. Gamage, 1987: Observations of turbulence in stratified flow. *J. Atmos. Sci.,* **44,** 1106–1121.

——, J. Sun, W. Blumen, A. Delaney, G. McClean, and S. Oncley, 1998: Nocturnal boundary-layer regimes. *Bound.-Layer Meteor.,* **88,** 255–278.

——, X. Lee, A. Black, H. Neumann, and R. M. Staebler, 2000: Vertical mixing in a partially open canopy. *Agric. For. Meteor.,* **101,** 67–78.

Merry, M., and H. A. Panofsky, 1976: Statistics of vertical motion over land and water. *Quart. J. Roy. Meteor. Soc.,* **102,** 255–260.

Moore, G. E., L. B. Milich, and M. K. Liu, 1988: Plume behaviors observed using lidar and SF6 tracer at a flat and hilly site. *Atmos. Environ.,* **22,** 1673–1688.

Moran, M., and R. A. Pielke, 1996: Evaluation of a mesoscale atmospheric dispersion modeling system with observations from the 1980 Great Plains Mesoscale Tracer Field Experiment. Part I: Datasets and meteorological simulations. *J. Appl. Meteor.,* **35,** 281–304.

Nasstrom, J., G. Sugiyama, J. Leone, and D. Ermak, 2000: A real-time atmospheric dispersion modeling system. Preprints, *11th Joint Conf. on the Applications of Air Pollution Meteorology*

with the A&WMA, Long Beach, CA, Amer. Meteor. Soc., 84–88.
Nieuwstadt, F. T. M., 1984: The turbulent structure of the stable, nocturnal boundary layer. *J. Atmos. Sci.,* **41,** 2202–2216.
Olesen, H. R., S. E. Larsen, and J. Hojstrup, 1984: Modeling velocity spectra in the lower part of the planetary boundary layer. *Bound.-Layer Meteor.,* **29,** 285–312.
Panofsky, H. A., and J. A. Dutton, 1984: *Atmospheric Turbulence—models and Methods for Engineering Applications.* John Wiley and Sons, 397 pp.
——, H. Tennekes, D. H. Lenschow, and J. C. Wyngaard, 1977: The characteristics of turbulent velocity components in the surface layer under convective conditions. *Bound.-Layer Meteor.,* **11,** 355–361.
Peltier, L., J. Wyngaard, S. Khanna, and J. Brasseur, 1996: Spectra in the unstable surface layer. *J. Atmos. Sci.,* **53,** 50–61.
Pilegaard, K., P. Hummelsjøj, N. O. Jensen, and Z. Chen, 2000: Contrasting the results from the first two seasons of continuous CO_2 eddy-flux measurements over a Danish beech forest. *Agric. For. Meteor.,* in press.
Riley, J. J., R. W. Metcalfe, and M. A. Weissman, 1981: Direct numerical simulations of homogeneous turbulence in density-stratified fluids. *Nonlinear Properties of Internal Waves,* B. J. West, Ed., American Institute of Physics, 79–112.
Rodean, H., 1996: *Stochastic Langrangian Models of Turbulent Diffusion. Meteor. Monogr.,* No. 48, Amer. Meteor. Soc., 84 pp.
Ruscher, P., and L. Mahrt, 1989: Coherent structures in the very stable atmospheric boundary layer. *Bound.-Layer Meteor.,* **47,** 41–54.
SethuRaman, S., 1977: The observed generation and breaking of atmospheric internal gravity waves over the ocean. *Bound.-Layer Meteor.,* **19,** 67–80.
Skupniewicz, C. E., 1987: Measurements of over water diffusion: The separation of relative diffusion and meander. *J. Climate Appl. Meteor.,* **26,** 949–958.
Smedman, A. S., 1988: Observations of a multi-level turbulence structure in a very stable atmospheric boundary layer. *Bound.-Layer Meteor.,* **44,** 231–253.
——, and U. Högström, 1975: Spectral gap in surface-layer measurements. *J. Atmos. Sci.,* **32,** 340–350.
Smith, B., and L. Mahrt, 1981: A study of boundary layer pressure adjustments. *J. Atmos. Sci.,* **38,** 334–346.
Sorbjan, Z., 1989: *Structure of the Atmospheric Boundary Layer.* Prentice Hall, 317 pp.
Stull, R. B., 1988: *An Introduction to Boundary Layer Meteorology.* Kluwer Academic, 666 pp.
Sun, J., 1999: Diurnal variation of thermal roughness height over a grassland. *Bound.-Layer Meteor.,* **92,** 407–427.
Vickers, D., and L. Mahrt, 1997: Quality control and flux sampling problems for tower and aircraft data. *J. Atmos. Oceanic Technol.,* **14,** 512–526.
Weinstock, J., 1980: A theory of gaps in the turbulence spectra of stably stratified shear flows. *J. Atmos. Sci.,* **37,** 1542–1549.
Wyngaard, J. C., 1973: On surface-layer turbulence. *Workshop on Micrometeorology,* D. A. Haugen, Ed., Amer. Meteor. Soc., 101–149.
——, and O. R. Coté, 1974: The evolution of a convective planetary boundary layer: A higher-order closure model study. *Bound.-Layer Meteor.,* **7,** 289–308.